



Dechlorination of 2,4-dichlorophenoxyacetic acid using biochar-supported nano-palladium/iron: Preparation, characterization, and influencing factors

Hongyi Zhou¹ | Ning Huang¹ | Yongkang Zhao¹ | Shams Ali Baig² | Junchao Xiang¹

¹College of Environment, Zhejiang University of Technology, Hangzhou, Zhejiang, 310014, China

²Department of Environmental Sciences, Abdul Wali Khan University, Mardan, 23200, Pakistan

Correspondence

Hongyi Zhou, College of Environment, Zhejiang University of Technology, Hangzhou, Zhejiang 310014, China.
Email: zhouhy@zjut.edu.cn

Funding information

National Natural Science Foundation of China, Grant/Award Number: 21477108

In the present study, peanut shell, a green waste raw material, was used to prepare biochar (BC) and to obtain BC-supported nano-palladium/iron (BC-nPd/Fe) composites for removing 2,4-dichlorophenoxyacetic acid (2,4-D) from water. Characterization analysis demonstrated that nPd/Fe particles were well dispersed on the BC surface with weakened magnetic properties. The average particle diameter and specific surface area of nPd/Fe were 101.3 nm and 6.7 m² g⁻¹, whereas the corresponding values of the BC-nPd/Fe materials were 88.8 nm and 14.8 m² g⁻¹, respectively. Several factors were found to influence the dechlorination of 2,4-D, including the weight ratio of BC to Fe, Pd loading ratio, initial solution pH, 2,4-D concentration, and reaction temperature. Dechlorination results indicated that the 2,4-D removal and phenoxyacetic acid (PA) generation rates were 44.1% and 20.1%, respectively, in the nPd/Fe system, and 100.0% and 92.1%, respectively, in the BC-nPd/Fe system. The dechlorination of 2,4-D was well described by the pseudo-first-order kinetic model ($R^2 > 0.97$), and the observed rate constants k_{obs} were 0.0042 min (nPd/Fe) and 0.0578 min (BC-nPd/Fe), respectively. The reaction mechanism indicated that the dechlorination hydrogenation was the main process to remove 2,4-D from water in the BC-nPd/Fe system. In addition, BC inhibited the formation of a passivation layer on the particle surface during the reaction, thus maintaining the high reactivity of BC-nPd/Fe. The easy preparation technique, high 2,4-D dechlorination capacity, and mild reaction conditions suggest that BC-nPd/Fe may be a promising alternative composite to remove 2,4-D from water.

KEYWORDS

2,4-D, biochar, Pd/Fe nanoparticles, reductive dechlorination

1 | INTRODUCTION

The chlorinated phenoxy herbicide 2,4-dichlorophenoxyacetic acid (2,4-D), a common plant growth regulator, has been extensively employed for

controlling broad-leafed weeds and increasing agriculture productivity in recent years.^[1] The most common trails of 2,4-D in the environment result from its direct application as herbicide or the wastewater generated during its manufacturing and transportation.^[2] Research reports

have shown that 2,4-D occurrence in the environment has different degrees of impact on human health and ecosystems.^[2,3] Generally, 2,4-D is both persistent and toxic, classified as an environmental endocrine disruptor and a carcinogenic substance.^[4–7] In addition, it has been reported that 2,4-D has been frequently detected in surface or groundwater worldwide because of its poor biodegradability and volatility.^[8] Therefore, effective treatments are required to efficiently remove 2,4-D from water.

At present, there are many technologies available for the remediation of chlorinated pollutants from aqueous systems, such as biological degradation,^[9] electroreductive dechlorination,^[10] advanced oxidation,^[11] adsorption,^[12,13] and nano-zero-valent iron (nZVI) reduction.^[14] Advanced oxidation technology and photocatalysis possess the advantages of short reaction time and high degradation efficiency, but the disadvantage associated with high-energy intensity.^[10,11] The energy consumption of any biodegradation technology is generally lower, but the selection and the acclimation of microbial communities are a long-term and complex work because of the toxicity of chlorinated contaminants.^[9] Adsorption and nZVI technology have become common methods for removing chlorinated pollutants from water environments owing to their environmental friendliness, ease of operation, and high efficiency.^[12,14] In practical applications, these two technologies are usually combined to achieve better processing results.

In recent years, nZVI has attracted wide attention because of its large surface area and high reaction properties.^[15] Generally, nZVI has a low redox potential of -0.44 V, which is usually used as an electron donor during the reduction process.^[15,16] Therefore, nZVI is extensively used to treat pollutants in water environments that contain chlorinated organics,^[16] heavy metals,^[17] organic dyes,^[18] and nitrates.^[19] However, as the reaction progresses, their reactivity for pollutants could be substantially reduced by the passivation layers (e.g., iron oxides and hydroxides) on the surface of nZVI.^[20] In addition, the passivation layer suppresses the electron transfer efficiency between zero-valent iron (ZVI, Fe^0) and pollutants.^[21] The reactivity of nZVI could be further enhanced by loading another noble metal (such as Pd,^[22,23] Ni,^[20,24] Cu,^[25] and Ag^[26]) on the nZVI surface. These noble metals can contribute to the formation of Fe-based bimetallic nanoparticles, of which the Pd/Fe nanoparticles exhibit the greatest reactivity. Thus, Pd/Fe nanoparticles have been widely utilized for the catalytic reduction of compounds, which typically have poor reactivity with nZVI.^[27–29] For instance, Zhuang et al.^[22] performed dechlorination

experiments on 2,3,4-trichlorobiphenyl (PCB 21) using nZVI (1 g) and nZVI/Pd (0.1 g with 0.25% Pd) for 20 and 70 days, respectively. The results indicated that palladization caused a dechlorination rate for PCB 21 500 times higher than before. In addition, Lien et al.^[30] pointed out that in the dechlorination experiments of trichloroethylene (TCE), the reactivity of the Pd/Fe nanoparticles (with 1% Pd) was approximately 70 times greater than that of the unpalladized nano-scale Fe particles.

The newly prepared Pd/Fe nanoparticles tended to quickly form large flocs or aggregates because of the magnetic attractions and van der Waals forces. Hence, their stability and reactivity in contaminated environments decreased as the reaction proceeded.^[31,32] In addition, the high surface energy of Pd/Fe nanoparticles leads to severe aggregation, which may reduce the reactivity.^[33] In order to solve the problem of easy agglomeration, many researchers have loaded nZVI or Pd/Fe nanoparticles on various functional materials to form composite materials. The common loaded matrices are activated carbon,^[34] silica,^[35] bentonite,^[36] multiwalled carbon nanotubes,^[37] metal oxides,^[38] and biochar (BC).^[39] Among them, the BC produced by pyrolysis of biomass under oxygen-limited or oxygen-free conditions has attracted research interest because it is considered to be a promising environmental remediation material.^[40]

Plant materials, woodchips, wood biomass, crop waste, carbon-rich organic biomass, and solid sludge waste are often considered as excellent raw materials for BC.^[41] BC has a porous structure and possesses a large surface area rich in diverse functional groups.^[42,43] BC can be successfully used to disperse and stabilize nanoparticles, thereby enhancing their performance in environmental applications.^[39] Wang et al.^[42] reviewed the preparation of BC from different raw materials and its capacity to remove various contaminants after loading nZVI. Qian et al.^[44] produced BC by pyrolyzing rice straw at different temperatures and loaded nZVI on the obtained composite to remove hexavalent chromium (Cr(VI)) in a water solution. Devi and Saroha^[45] synthesized BC (prepared from paper mill sludge) Ni-ZVI-combined magnetic materials (Ni-ZVI-MBCs), which were utilized as an adsorbent to remove pentachlorophenol (PCP) from wastewater. These studies focused on the simultaneous adsorption and reduction of pollutants by BC-supported nZVI or bimetals. Nevertheless, few studies have reported the removal of chlorinated organic pollutants by BC-supported iron-based bimetal particles.^[46,47] Therefore, it is of great significance to investigate BC composites that can efficiently reduce chlorinated organic contaminants from water under different environmental conditions.^[48,49]

Peanut shells are usually regarded as food by-products that are normally discarded in the food industry and agriculture.^[50] Owing to its porous structure, the peanut shell could become an excellent supporting material for nZVI or bimetal. In the present study, a peanut shell was used as the raw material of BC to synthesize BC-supported nano-palladium/iron (BC-nPd/Fe), a new composite material for the effective dechlorination of 2,4-D in water. In addition, the effects of reaction parameters on 2,4-D dechlorination by BC-nPd/Fe were explored, and the reaction mechanism of 2,4-D dechlorination by BC-nPd/Fe was further discussed by characterizing the material properties and investigating the reductive dechlorination process.

2 | MATERIALS AND METHODS

2.1 | Materials

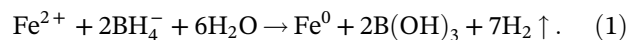
The 2,4-D ($C_8H_6Cl_2O_3$, 98%), 2-chlorophenoxyacetic acid (2-CPA, $C_8H_7ClO_3$, >98%), 4-chlorophenoxyacetic acid (4-CPA, $C_8H_7ClO_3$, >98%), and phenoxyacetic acid (PA, $C_8H_8O_3$, 98%) were purchased from Alfa Aesar (Tianjin, China). Sodium borohydride ($NaBH_4$, ≥97%), ferrous sulfate ($FeSO_4 \cdot 7H_2O$, 99–101%), ethanol (CH_3CH_2OH , >99.7%), and methanol (CH_3OH , 99.5%) were obtained from Sinopharm Chemical Regent Co., Ltd. (Shanghai, China). Potassium hexachloropalladate (K_2PdCl_6 , 99%) was purchased from Macklin Biochemical Co., Ltd. (Shanghai, China). Methanol (CH_3OH , high-performance liquid chromatography [HPLC] grade) was purchased from Tedia Company Inc. (Shanghai, China). Deionized (DI) water, previously deoxygenated by bubbling N_2 gas for 1.0 h, was used in all the experiments.

2.2 | Preparation of BC-nPd/Fe

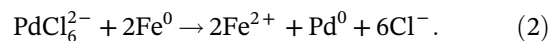
The BC precursor material, peanut shells, was obtained from a local market in Hangzhou City, China. Briefly, peanut shells were smashed and passed through a 150-mesh screen and then calcined at 500°C for 3.0 h in a tube furnace at a heating rate of 10.0°C min^{-1} under nitrogen (N_2) flow (100.0 ml min^{-1}).

The BC-nPd/Fe was synthesized in a three-necked flask under mechanical stirring (200 r min^{-1}) under N_2 atmosphere. First, BC was added to 400.0 ml of $FeSO_4 \cdot 7H_2O$ solution and sonicated for 30.0 min to ensure that the BC was evenly dispersed in the solution. Next, 80.0 ml of $NaBH_4$ solution was added dropwise to the solution (the molar ratio of BH_4^-/Fe^{2+} was 2.0).

BC-supported nZVI (BC-nZVI) was formed, and the reaction can be depicted as Equation 1:



A 10.0 ml of K_2PdCl_6 solution was added to the BC-nZVI solution after 30.0 min. Then, Pd^{2+} was reduced by Fe^0 , resulting in a BC-nPd/Fe solution according to Equation 2:



After 60.0 min of continuous reaction, BC-nPd/Fe particles were separated by an externally enhanced magnetic field, washed three times with oxygen-free DI water and ethanol, and then collected by drying in a vacuum oven at 60°C for 6.0 h. The synthesis steps of nPd/Fe are consistent with the aforementioned methods. In this study, the Pd loading (weight ratio of Pd to Fe) was calculated using Equation 3:

$$Pd/Fe(\%) = \frac{M_{Pd}}{M_{Fe}} = \frac{M_{K_2PdCl_6} \times 26.78\%}{M_{Fe}}. \quad (3)$$

2.3 | Batch experiments

Batch experiments of 2,4-D dechlorination were performed in a three-necked flask immersed in a constant-temperature water bath. The 2,4-D solutions and a certain amount of DI water were added to the flask containing freshly prepared nPd/Fe or BC-nPd/Fe particles to 500.0 ml of total reaction volume. The reaction solution was continuously stirred ($n = 200$ r min^{-1}) under an N_2 atmosphere. The effects of 2,4-D dechlorination by BC-nPd/Fe under different experimental conditions ($M_{BC}:M_{Fe}$ [weight ratio of BC to Fe], Pd loading, initial pH, initial 2,4-D concentration, and reaction temperature) were investigated. The reaction solution was sampled at different reaction time intervals, passed through a 0.22- μm microporous membrane and stored in a sample vial for HPLC analysis. Samples were processed in triplicate, and the mean values were used for the analysis.

2.4 | Characterization analyses

The Brunauer–Emmett–Teller (BET) surface areas of nPd/Fe and BC-nPd/Fe were measured using an N_2 adsorption method with a surface analyzer (ASAP2020M,

Micromeritics Instrument Corp., USA). The surface morphology of the sample was analyzed by scanning electron microscopy (SEM, S4700, Hitachi, Japan), and the surface element distribution of the material was analyzed by energy dispersive spectroscopy (EDS, NSS7, Thermo Fisher Scientific, China). X-ray diffraction (XRD) spectra of the materials were recorded with X'Pert PRO (PANalytical, Netherlands) using K radiation over the 5–80° scan range. Magnetic characterization was performed using a vibrating sample magnetometer (VSM, VersaLab, USA) instrument between a magnetic field from –15,000 to 15,000 Oe. Fourier transform infrared (FTIR) spectra were collected using an IRTracer-100 spectrometer in the wavenumber range of 4,000–500 cm⁻¹. Thermogravimetric analyses (TGAs) were conducted on a TGA 4000 analyzer (PerkinElmer, USA) from 30°C to 800°C at a heating rate of 10.0°C min⁻¹ under an N₂ atmosphere. The surface compositions of the samples were analyzed by X-ray photoelectron spectroscopy (XPS, Kratos AXIS Ultra DLD, Shimadzu Ltd, Japan).

2.5 | Analytical methods

The concentration of organic matter (2,4-D, PA, 2-CPA, and 4-CPA) in aqueous solution were quantified using HPLC (Agilent Technologies 1200 Series, USA) equipped with an Eclipse XDB-C18 HPLC column (150 mm × 4.6 mm; I.D. 5 μm Agilent, USA), and an ultraviolet detector (UVD) operated at a wavelength of 210 nm.^[51] Methanol/ultrapure water (60/40, v/v) was selected as the HPLC mobile phase (pH was adjusted to 3.0 by adding 0.5 mol L⁻¹ H₃PO₄) at a flow rate of 1.0 ml min⁻¹ with an injection volume of 20 μl. The column temperature was set at 30°C, and the total analysis time was 10.0 min. The pseudo-first-order kinetic model^[30] was applied to describe the dechlorination of 2,4-D, which can be represented by the following equation:

$$\frac{dC}{dt} = -k_{\text{obs}}C, \quad (4)$$

where C is the 2,4-D concentration (mg L⁻¹) in the aqueous solution at time t (min) and k_{obs} is the observed pseudo-first-order kinetic rate constant (min).

3 | RESULTS AND DISCUSSION

3.1 | Characterization analysis results

Figure 1 presents the surface morphology and particle size distribution of nPd/Fe and BC-nPd/Fe. The results

indicate that the nPd/Fe particles are interconnected by a chain structure and agglomeration, as shown in Figure 1a. The average particle diameter was 101.3 nm (Figure 1b). Such aggregation could be explained by the severe magnetic attractions and van der Waals forces interaction between the particles. The agglomeration of the nPd/Fe particles decreased the reactivity because the surface reaction sites were covered by other particles.^[33] In contrast, more dispersed nPd/Fe particles were clearly observed on the surface of the BC-nPd/Fe material (Figure 1c). Moreover, the average diameter of these particles decreased to 88.8 nm (Figure 1d).

Figure 2a presents the N₂ adsorption–desorption isotherms. The specific surface areas of nPd/Fe and BC-Pd/Fe calculated were 6.7 and 14.8 m² g⁻¹, respectively. The VSM characterization of nPd/Fe and BC-nPd/Fe is illustrated in Figure 2b. The hysteresis loops of both materials were typically S-like curves, and the intensity of the saturation magnetization values were 2.35 and 0.64 emu mg⁻¹ for nPd/Fe and BC-nPd/Fe, respectively. Compared with nPd/Fe, the lower magnetic saturations of BC-nPd/Fe could be attributed to the introduction of BC. The SEM, BET, and VSM characterization results indicated that the presence of BC reduced the intensive magnetic attraction between nPd/Fe particles, thereby suppressing the agglomeration between these nanoparticles. The dispersion of nPd/Fe particles with smaller size on the surface of BC means that BC-Pd/Fe composites possess more active reaction sites and larger contact area with contaminants, which is conducive to the reductive dechlorination of 2,4-D.

The FTIR spectra of BC, nPd/Fe, and BC-nPd/Fe are shown in Figure 3a. The bands around 1,490 cm⁻¹ represented the stretching vibration of aromatic C=O and benzene ring C=C, and the band at 750 cm⁻¹ was assigned to the bending vibration of C–H and O–H.^[43] The absorption peaks at 1,100–900 and 553 cm⁻¹ were ascribed to the Fe–O stretch vibration.^[3,38] These characteristic peaks can be clearly observed on BC-nPd/Fe, indicating that nPd/Fe was successfully loaded on the BC. TGAs of BC, nPd/Fe, and BC-nPd/Fe are shown in Figure 3b. The weight loss of BC below 250°C was due to the desorption of water and small organic molecules. As the temperature increased, the organic structure in the BC decomposed, with a total weight loss of 31.7% at 800°C.^[40] The mass of the nPd/Fe material increased to 120.5% of the original sample at 800°C, which may be attributed to the thermal decomposition of iron oxides (which was verified by XPS) under high-temperature conditions.^[27] The BC-nPd/Fe composites slowly lost weight below 450°C, with a maximum mass loss of 2.9%. The sample gradually gained weight in the temperature range of 450–650°C; then, its weight almost reached

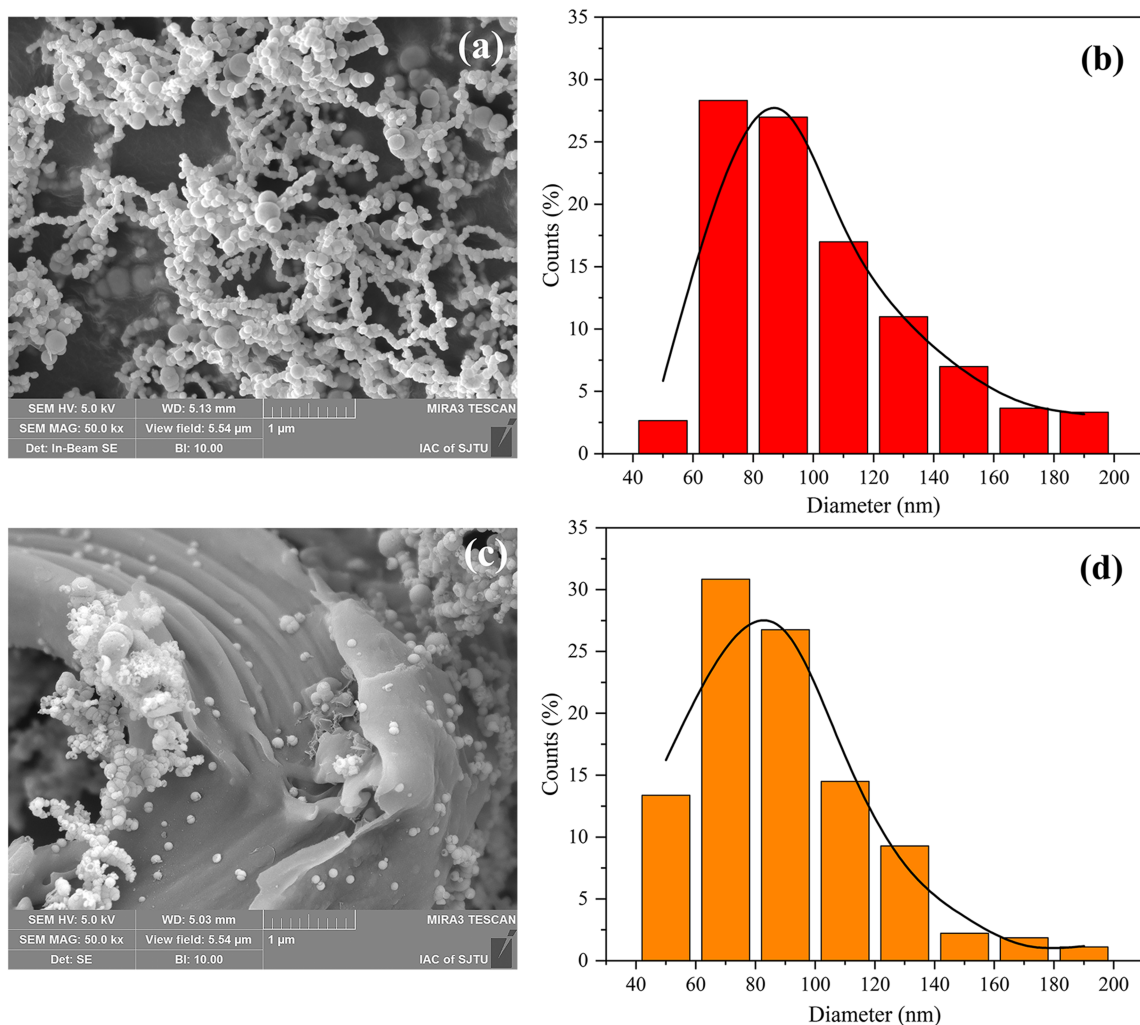


FIGURE 1 SEM images of (a) nPd/Fe and (c) BC-nPd/Fe; (b) and (d) are the particle size distribution histograms to (a) and (c). BC-nPd/Fe, biochar-supported nano-palladium/iron; SEM, scanning electron microscopy

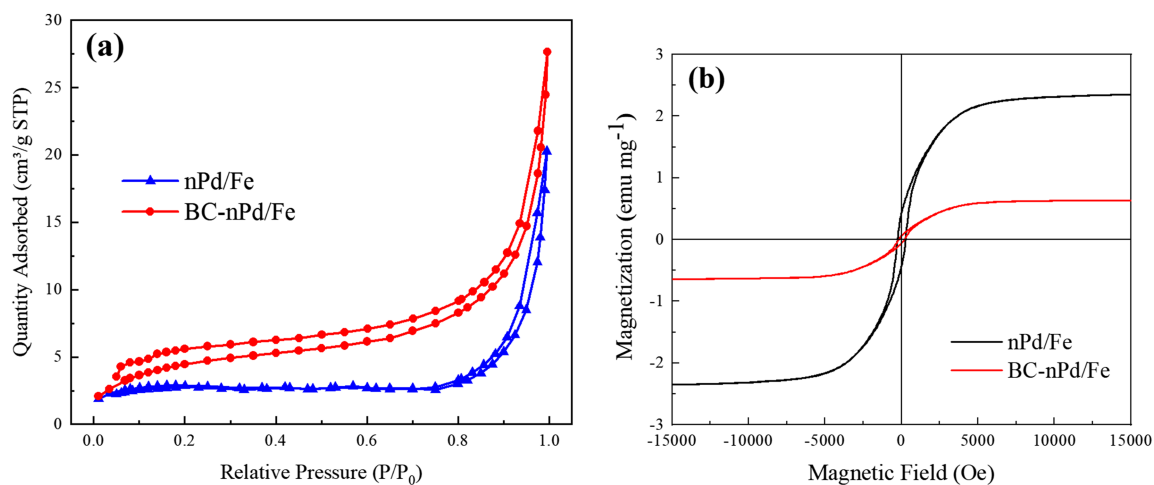


FIGURE 2 (a) N_2 adsorption-desorption isotherms and (b) magnetization curves of nPd/Fe and BC-nPd/Fe. BC-nPd/Fe, biochar-supported nano-palladium/iron

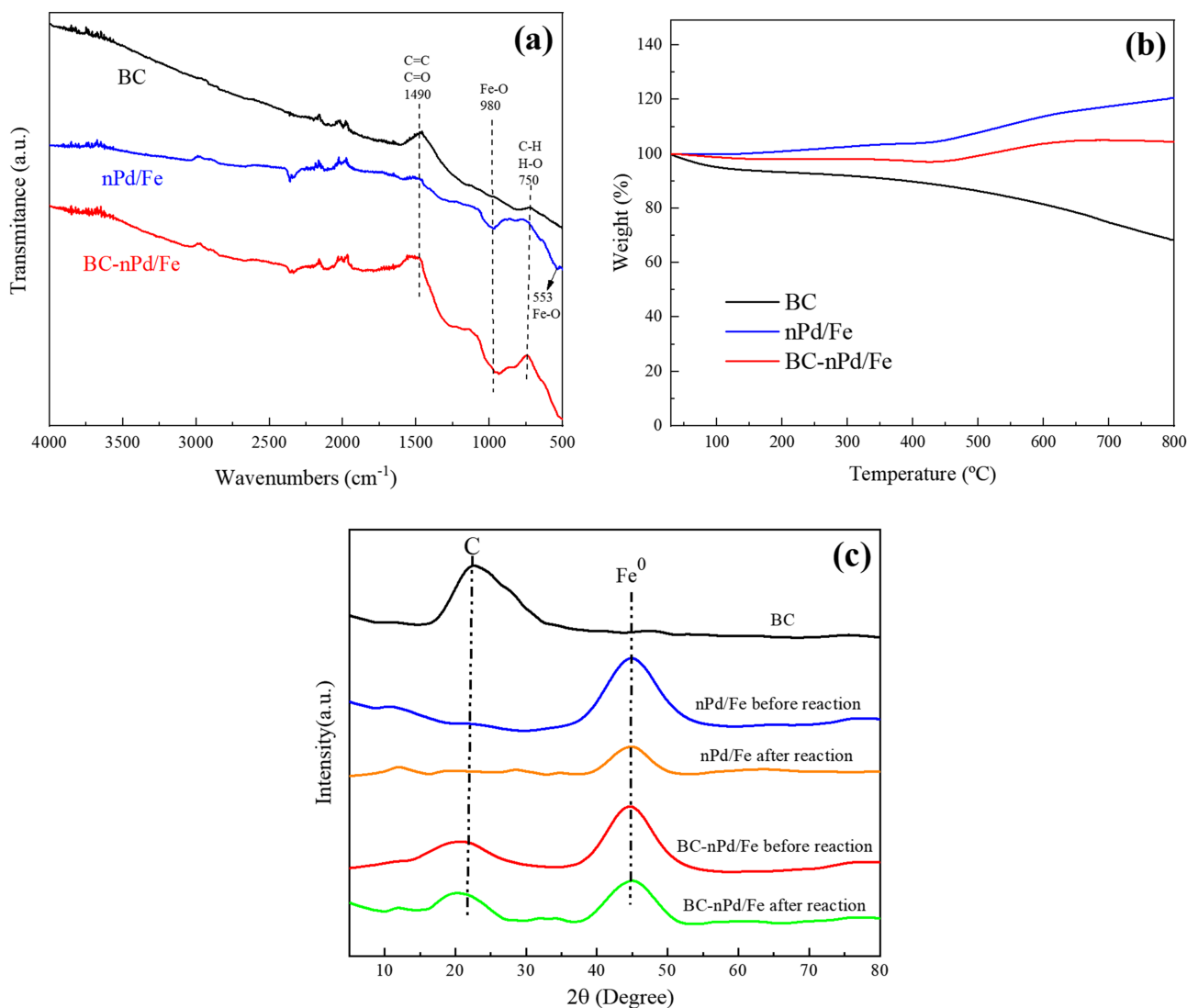


FIGURE 3 (a) FTIR spectra, (b) thermogravimetric curves, and (c) X-ray diffraction patterns of BC, nPd/Fe, and BC-nPd/Fe. BC-nPd/Fe, biochar-supported nano-palladium/iron; FTIR, Fourier transform infrared

equilibrium, with a final weight 104.4% of that of the original sample. The results further indicated that nPd/Fe was successfully supported on BC, and the BC-nPd/Fe composites remained stable between 650°C and 800°C in an N₂ atmosphere. The XRD patterns of BC, nPd/Fe, and BC-nPd/Fe are shown in Figure 3c. The characteristic peak of carbon ($2\theta = 22.7^\circ$)^[52] can be clearly observed in BC. The peak at $2\theta = 44.7^\circ$ was the typical diffraction peak of ZVI (Fe⁰),^[44] which was clearly observed in the XRD patterns of nPd/Fe and BC-nPd/Fe before the reaction. The characteristic peaks for both carbon and Fe⁰ appearing in the BC-nPd/Fe suggest that the composites were successfully synthesized. However, after the reaction, a significant Fe⁰ peak was observed again in BC-nPd/Fe, sharply contrasting with the faint Fe⁰ peak intensity of nPd/Fe. A possible explanation is that BC

inhibited the formation of the passivation layer during the reaction so that the Fe⁰ was exposed on the surface of the particles, thereby maintaining the reactivity of BC-nPd/Fe. It is difficult to observe the characteristic peaks of Pd in the XRD patterns because of the extremely low Pd content in the materials.

The local element information of the BC-nPd/Fe materials before and after the reaction was determined by EDS. As shown in Figure 4, the elements on the surface of BC-nPd/Fe are mainly composed of C, Fe, O, and Pd. The layered image further confirmed that the nPd/Fe particles were dispersed on the BC surface. In comparison, the O weight ratio increased from 9.51% to 19.82%, whereas the Fe weight ratio decreased from 26.25% to 22.04% on the surface of the BC-nPd/Fe after the reaction. The results indicated that iron was oxidized during

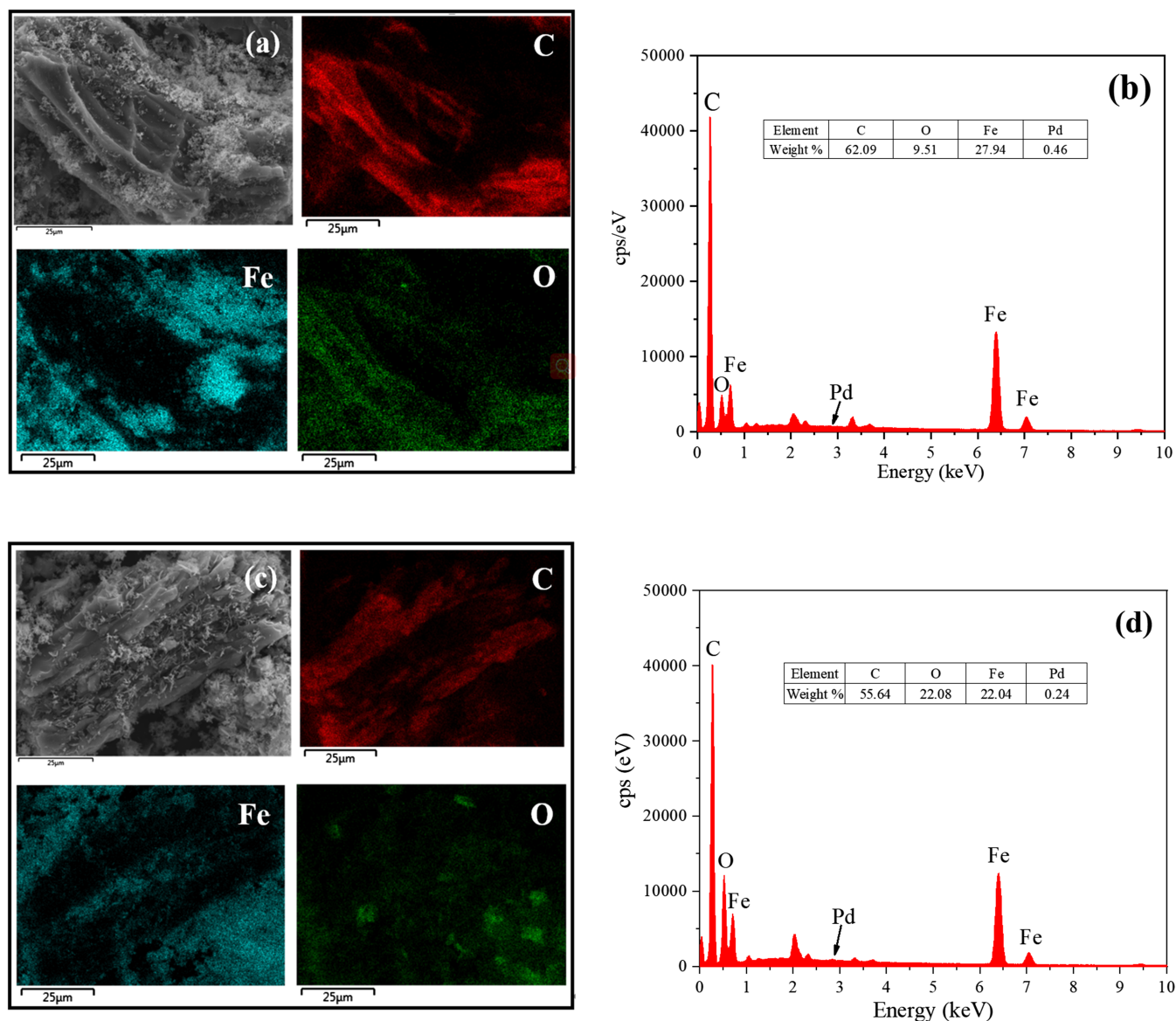


FIGURE 4 Elemental mappings of BC-nPd/Fe (a) before and (c) after reaction; (b) and (d) are the EDS spectrums to (a) and (c). BC-nPd/Fe, biochar-supported nano-palladium/iron; EDS, energy dispersive spectroscopy

the reaction to form a passivation layer covering the surface of the material.

The XPS analyses for Fe 2p and Pd 3d before and after the nPd/Fe and BC-nPd/Fe reactions are shown in Figure 5. The XPS of Fe 2p shows that the two broad peaks at 710.9 and 724.1 eV represent Fe 2p_{3/2} and Fe 2p_{1/2}, respectively, which imply that Fe oxides or hydroxides (Fe—O_x, Fe(OH)₃, and FeOOH) are present on the surface of these particles (Figure 5a,c).^[14,37,53] The characteristic peak at 706.9 eV corresponds to the binding energy of Fe⁰.^[37] As shown in Figure 5b,d, the Pd 3d_{5/2} and Pd 3d_{3/2} photoelectron peaks are located at 335.2 and 340.3 eV, respectively.^[51] The contents of Fe⁰ and Pd⁰ in the fresh nPd/Fe particles were 13.0% and 59.9%,

respectively, and the values were 15.3% and 81.0% in the fresh BC-nPd/Fe materials, respectively. The BC-nPd/Fe particles with higher content of reducing agent (Fe⁰) and catalyst (Pd⁰) displayed greater reactivity at the beginning of the reaction, after which, the contents of Fe⁰ and Pd⁰ on the surface of the nPd/Fe particles decreased to 4.6% and 39.0%, respectively. The results suggested that nZVI was oxidized to form a passivation layer (Equations 5 and 6) covering the surface of the particles during the reaction, and Pd⁰ as the catalyst was also quickly consumed, resulting in a decrease in the reaction activity of nPd/Fe. Compared with nPd/Fe, BC-nPd/Fe particles maintained a higher Fe⁰ (11.3%) and Pd⁰ (48.3%) content after the reaction, indicating that the presence of BC

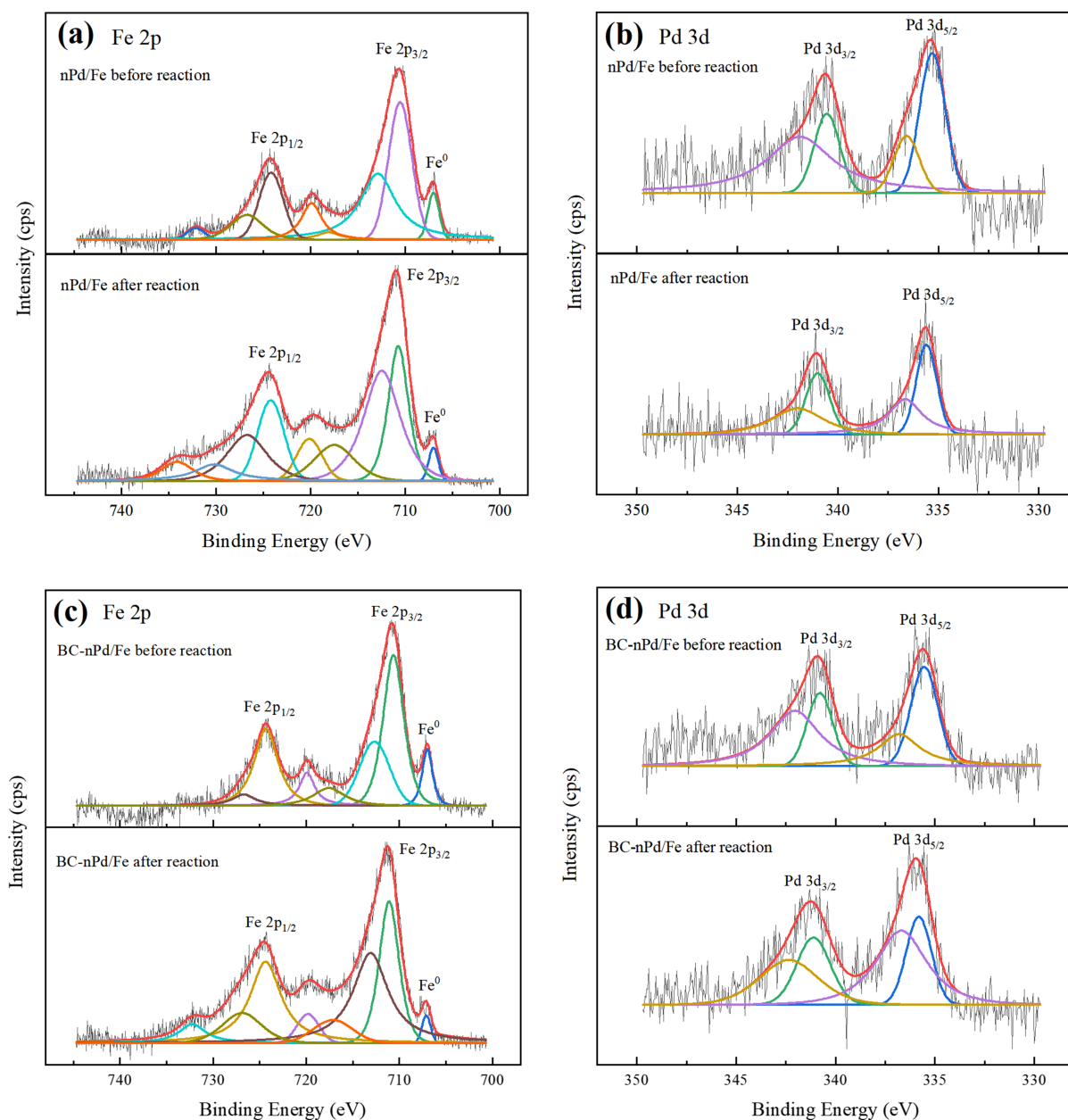
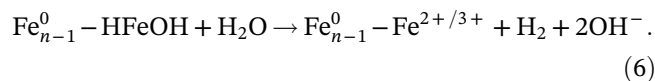
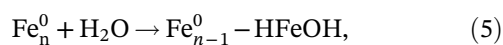


FIGURE 5 XPS spectra for (a) Fe2p of nPd/Fe, (b) Pd3d of nPd/Fe, (c) Fe2p of BC-nPd/Fe, and (d) Pd3d of BC-nPd/Fe. BC-nPd/Fe, biochar-supported nano-palladium/iron; XPS, X-ray photoelectron spectroscopy

effectively hindered the passivation layer generated (the passivation layer present on the surface of the nPd/Fe particles was thinner), so that more Fe and Pd were detected on the surface of the materials. In addition, the thinner passivation layer was beneficial to the reaction of nZVI corrosion and H_2 dissociation. Therefore, the carrier BC retained the high reduction reactivity of nPd/Fe, which was conducive to the dechlorination of 2,4-D by BC-nPd/Fe.



3.2 | Factors affecting 2,4-D dechlorination by BC-nPd/Fe

3.2.1 | Effect of $M_{BC}:M_{Fe}$

Figure 6 shows the effect of $M_{BC}:M_{Fe}$ on 2,4-D dechlorination. The nZVI content (1.0 g L^{-1}) was controlled and the quantity of BC was changed to obtain BC-nPd/Fe

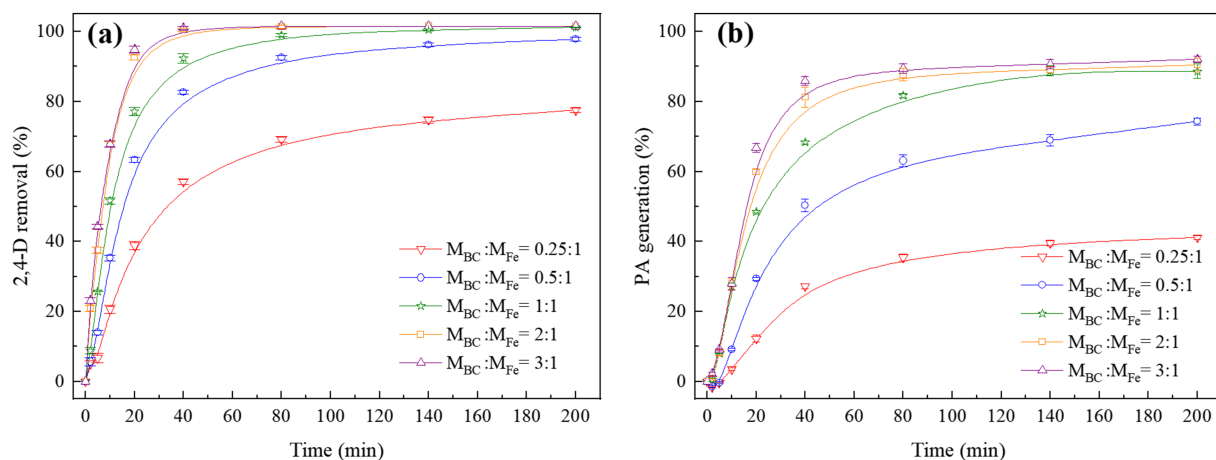


FIGURE 6 Effect of weight ratio of BC to Fe on dechlorination of 2,4-D by BC-nPd/Fe ($nZVI = 1.0 \text{ g L}^{-1}$, $C_{0,2,4-D} = 20.0 \text{ mg L}^{-1}$, $Pd/Fe = 0.5\%$, $pH = 7.0$, $T = 25.0^\circ\text{C}$, $n = 200 \text{ r min}^{-1}$). 2,4-D, 2,4-dichlorophenoxyacetic acid; BC-nPd/Fe, biochar-supported nano-palladium/iron; nZVI, nano-zero-valent iron

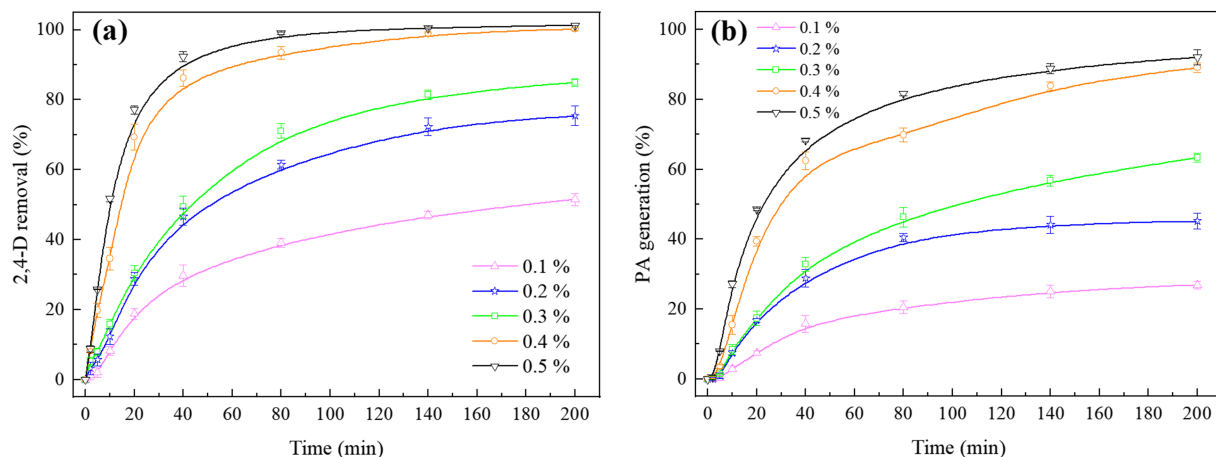


FIGURE 7 Effect of Pd loading on 2,4-D dechlorination by BC-nPd/Fe ($nZVI = 1.0 \text{ g L}^{-1}$, $C_{0,2,4-D} = 20.0 \text{ mg L}^{-1}$, $pH = 7.0$, $T = 25.0^\circ\text{C}$, $M_{BC}:M_{Fe} = 1:1$, $n = 200 \text{ r min}^{-1}$). 2,4-D, 2,4-dichlorophenoxyacetic acid; BC-nPd/Fe, biochar-supported nano-palladium/iron; nZVI, nano-zero-valent iron

materials with different $M_{BC}:M_{Fe}$ ratios (0.25:1, 0.5:1, 1:1, 2:1, and 3:1, respectively). At higher $M_{BC}:M_{Fe}$ ratios ($\geq 1:1$), 2,4-D was completely removed by BC-nPd/Fe (Figure 6a), whereas the phenoxyacetic acid (PA) generation was higher than 88% (Figure 6b) after 200 min of reaction. The results showed that BC-nPd/Fe composites with a high $M_{BC}:M_{Fe}$ ratio had a significant dechlorination effect on 2,4-D. In contrast, BC-nPd/Fe with an $M_{BC}:M_{Fe}$ ratio of 0.25:1 had a poor dechlorination effect on 2,4-D. The possible reason may be that the nPd/Fe particles cannot be sufficiently dispersed on the material surface with low BC content. When the $M_{BC}:M_{Fe}$ ratio was greater than 1:1, the PA generation rate increased slightly, which was 90.5% ($M_{BC}:M_{Fe} = 2:1$) and 92.1% ($M_{BC}:M_{Fe} = 3:1$). Based on the aforementioned

results, an $M_{BC}:M_{Fe}$ ratio of 1:1 was chosen for further experiments.

3.2.2 | Effect of Pd loading

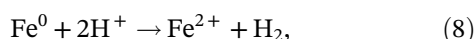
Pd loading had a significant effect on the dechlorination of 2,4-D (Figure 7). The 2,4-D removal rate increased from 51.5% to 100.0% with an increase in Pd loading (from 0.1% to 0.5%) (Figure 7a). The increasing trend of the PA generation rate (from 26.9% to 92.1%) was more obvious, and resultantly the higher Pd loading, the higher dechlorination efficiency. During the reaction, H_2 was generated due to the corrosion of nZVI (Equations 7 and 8). The generated H_2 was quickly adsorbed by Pd (a good

catalyst^[30]) and converted into strongly reducible hydrogen (H^*) (Equation 9), facilitating the hydrodechlorination of 2,4-D. Therefore, sufficient Pd loading can produce the reducible H^* required for the reaction in time. In addition, metal Pd as a catalyst reduces the activation energy,^[48] so the dechlorination reaction of 2,4-D is more likely to occur. Moreover, it is generally believed that metal Pd could form a galvanic cell with ZVI.^[54] More efficient electron transfer between BC-nPd/Fe and 2,4-D at high Pd loading ratios may be one of the reasons for the effective improvement of the dechlorination efficiency of 2,4-D.

Neutral or alkaline conditions:



Acidic conditions:



3.2.3 | Effect of initial solution pH

The pH value is a critical factor in the reduction of organics.^[55] As shown in Figure 8, 2,4-D was completely removed with an increase in initial pH from 5.0 to 7.0, whereas the PA production decreased from 92.7% to 89.4%. This insignificant change is attributed to the fact that ZVI could produce more corrosion in acidic solutions, so BC-nPd/Fe could maintain excellent dechlorination performance for 2,4-D. When the initial pH

increased to 8.5, the 2,4-D removal and PA generation rate decreased to 75.1% and 29.9%, respectively. The remarkable decline (particularly of PA generation, as shown in Figure 8b) could be explained by the following reasons. First, the OH^- concentration in the solution increased with increasing initial pH value. A large amount of OH^- reacts easily with free iron ions to form a passivation layer, which covers the surface of the nPd/Fe particles and hinders the corrosion of nZVI. Second, the passivation layer also hindered the contact of 2,4-D with the BC-nPd/Fe surface reaction sites and thus suppressed the dechlorination reaction. On the contrary, H^+ in the solution could dissolve the passivation layer and make the corrosion reaction of nZVI to easily occur, which facilitates the dechlorination of 2,4-D. Third, 2,4-D carries negative charges in an alkaline solution.^[23] Because of the negative surfaces of BC,^[42] the electrostatic repulsion between BC and 2,4-D resulted in a decreased dechlorination efficiency of BC-nPd/Fe for 2,4-D. In general, 2,4-D removal and PA generation (which varied with the initial pH values) did not change significantly under acidic or neutral conditions ($pH \leq 7.0$), whereas the downward trend gradually became apparent in an alkaline environment ($pH > 7.0$). For example, the PA generation at an initial pH of 7.0 was 82.4%, which was 2.76 times that at pH 8.5. Hence, it can be considered that an alkaline reaction environment is more detrimental to 2,4-D dechlorination.

3.2.4 | Effect of initial 2,4-D concentration

The effect of initial 2,4-D concentration on the dechlorination efficiency was evaluated, and the results are shown in Figure 9. The 2,4-D removal rate after

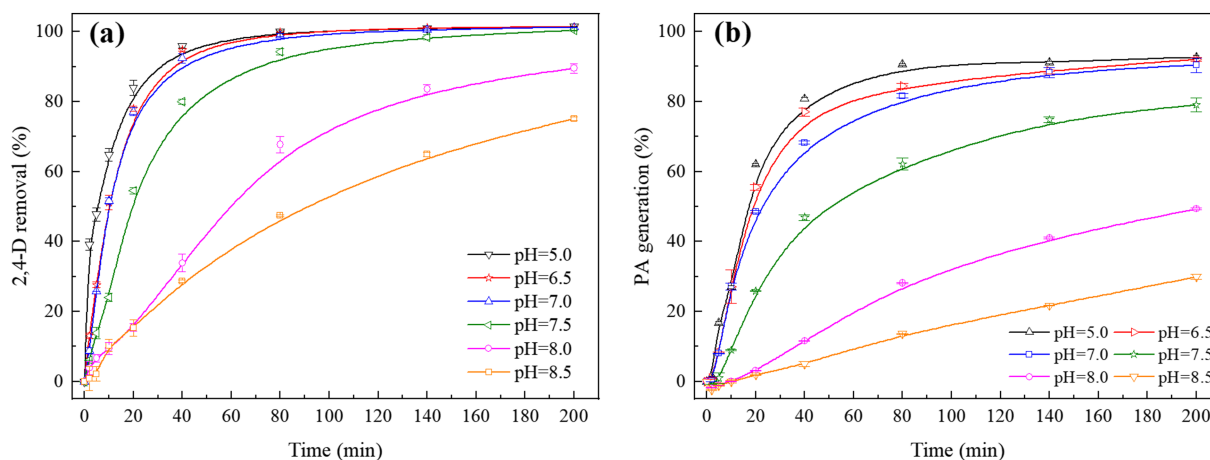


FIGURE 8 Effect of initial pH on 2,4-D dechlorination by BC-nPd/Fe. (nZVI = 1.0 g·L⁻¹, C_{0, 2,4-D} = 20.0 mg L⁻¹, Pd/Fe = 0.5%, T = 25.0°C, M_{BC}:M_{Fe} = 1:1, n = 200 r min⁻¹), 2,4-D, 2,4-dichlorophenoxyacetic acid; BC-nPd/Fe, biochar-supported nano-palladium/iron; nZVI, nano-zero-valent iron

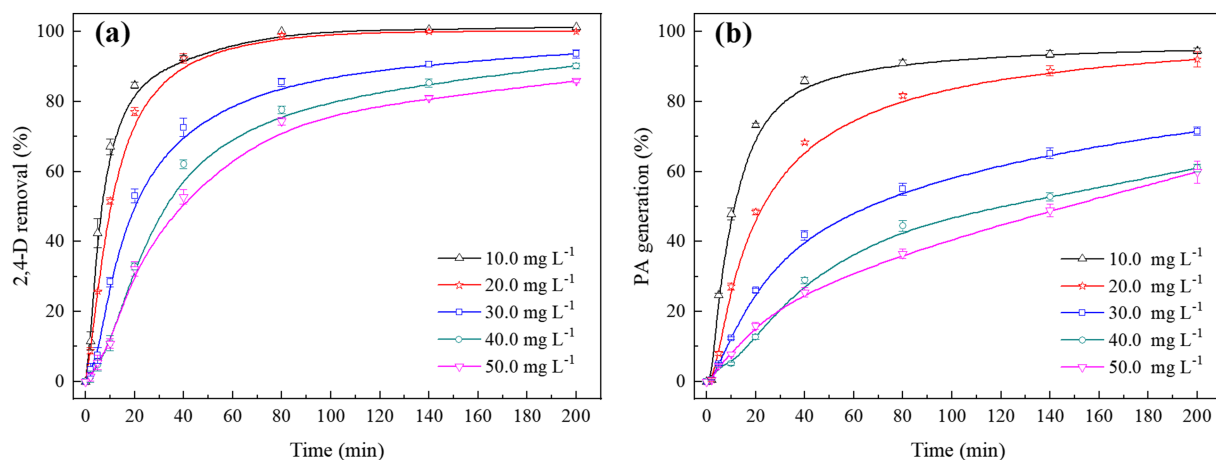


FIGURE 9 Effect of initial 2,4-D concentration on 2,4-D dechlorination by BC-nPd/Fe ($nZVI = 1.0 \text{ g L}^{-1}$, $C_{0,2,4-D} = 20.0 \text{ mg L}^{-1}$, $\text{pH} = 7.0$, $\text{Pd/Fe} = 0.5\%$, $T = 25.0^\circ\text{C}$, $M_{\text{BC}}:M_{\text{Fe}} = 1:1$, $n = 200 \text{ r min}^{-1}$). 2,4-D, 2,4-dichlorophenoxyacetic acid; BC-nPd/Fe, biochar-supported nano-palladium/iron; nZVI, nano-zero-valent iron

200.0 min was 100.0%, 100.0%, 93.7%, 90.2%, and 85.9% when the concentrations of 2,4-D were 10.0, 20.0, 30.0, 40.0, and 50.0 mg L^{-1} , respectively (Figure 9a). Additionally, the PA generation rates were 94.5%, 92.1%, 71.5%, 61.0%, and 59.9%, respectively (Figure 9b). The results showed that the dechlorination efficiency of BC-nPd/Fe for 2,4-D decreased with an increase in the initial 2,4-D concentration. Interestingly, a lower initial concentration of 2,4-D (10.0–20.0 mg L^{-1}) was rapidly adsorbed by the surface reaction site and then reduced by BC-nPd/Fe, resulting in greater 2,4-D removal and PA generation. Simultaneously, the reaction sites of the composites were fully utilized. However, the concentration of 2,4-D continued to increase, and BC-nPd/Fe did not have sufficient reaction sites for the dechlorination of 2,4-D, leading to a reduction in dechlorination efficiency. In addition, as the reaction proceeded, the competitive adsorption between the dechlorinated product and 2,4-D also reduced the reaction rate.^[41,44]

3.2.5 | Effect of reaction temperature

The effects of reaction temperature on the dechlorination of 2,4-D were investigated at 20.0°C, 25.0°C, 30.0°C, 35.0°C, and 40.0°C, as shown in Figure 10. When the reaction temperature increased from 20.0°C to 25.0°C, 2,4-D complete removal rates (100.0%) were observed, and the PA generation increased from 89.1% to 92.1%. Increasing the temperature accelerated the molecular movement, which was conducive to the diffusion of 2,4-D to the surface of BC-nPd/Fe, but the enhancement of the 2,4-D dechlorination reaction was limited to the above conditions. As the temperature continued to increase, significant reductions in both 2,4-D removal

and PA generation were observed. When the reaction temperature was increased to 40.0°C, the 2,4-D removal rate decreased to 34.4%, and the PA generation rate was only 10.1% (Figure 10a). 2,4-D molecules can easily move to the surface of the nanoparticles at higher temperatures, but excessive temperature could accelerate the oxidation of nZVI and form a passivation layer to cover the reaction sites,^[28,29] thus reducing the dechlorination ability of BC-nPd/Fe to 2,4-D. In summary, 25.0°C was the optimal reaction temperature recorded in the present study.

3.3 | Dechlorination process and kinetics of 2,4-D by nPd/Fe and BC-nPd/Fe

Figure 11 shows the progress of 2,4-D dechlorination by nPd/Fe and BC-nPd/Fe. In the nPd/Fe system (Figure 11a), 2,4-D removal rate was 44.1%, and PA generation rate was 20.1% at a reaction time of 200 min. At the same reaction time, 2,4-D was completely removed by BC-nPd/Fe, whereas 92.1% of PA was generated (Figure 11b). The experimental results showed that BC loading significantly promoted the dechlorination of 2,4-D by nPd/Fe. In both systems, the 2,4-D dechlorination products were 2-CPA and PA, but the intermediate 4-CPA was not detected. During the entire dechlorination process, almost all 2,4-D was first converted to 2-CPA (instead of 4-CPA) and then reduced to PA. The main reason for this may be the steric effect of the oxygen-containing functional group in the 2,4-D molecule, making the para-chlorine atom more easily replaced by hydrogen.^[22] It can be observed that the concentration of 2-CPA reaches a peak within 10–20 min and then decreases slowly (Figure 11b). Zhou et al.^[23] also pointed

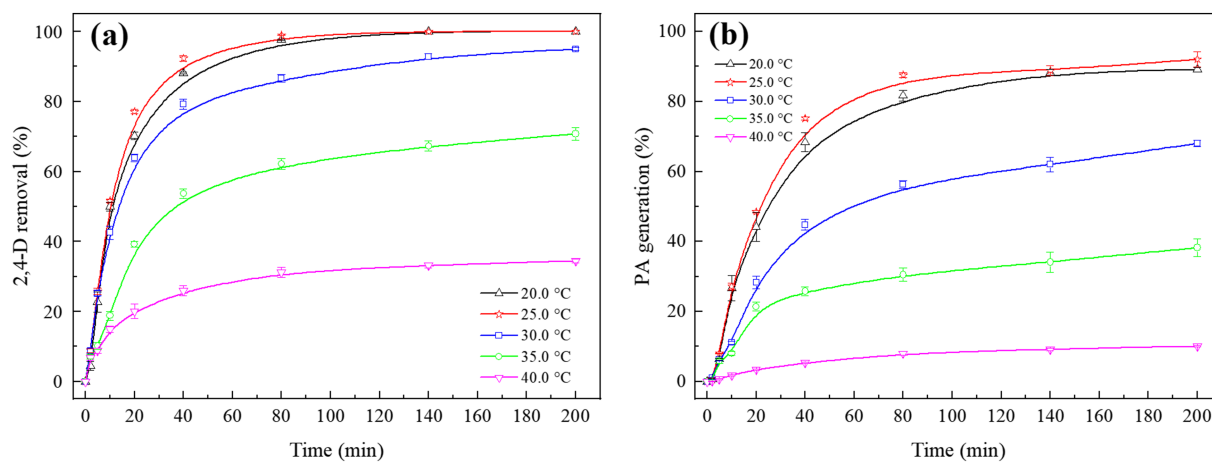


FIGURE 10 Effect of reaction temperature on 2,4-D dechlorination by BC-nPd/Fe ($nZVI = 1.0 \text{ g L}^{-1}$, $C_{0,2,4-D} = 20.0 \text{ mg L}^{-1}$, $\text{pH} = 7.0$, $\text{Pd/Fe} = 0.5\%$, $M_{\text{BC}}:M_{\text{Fe}} = 1:1$, $n = 200 \text{ r min}^{-1}$). 2,4-D, 2,4-dichlorophenoxyacetic acid; BC-nPd/Fe, biochar-supported nano-palladium/iron; nZVI, nano-zero-valent iron

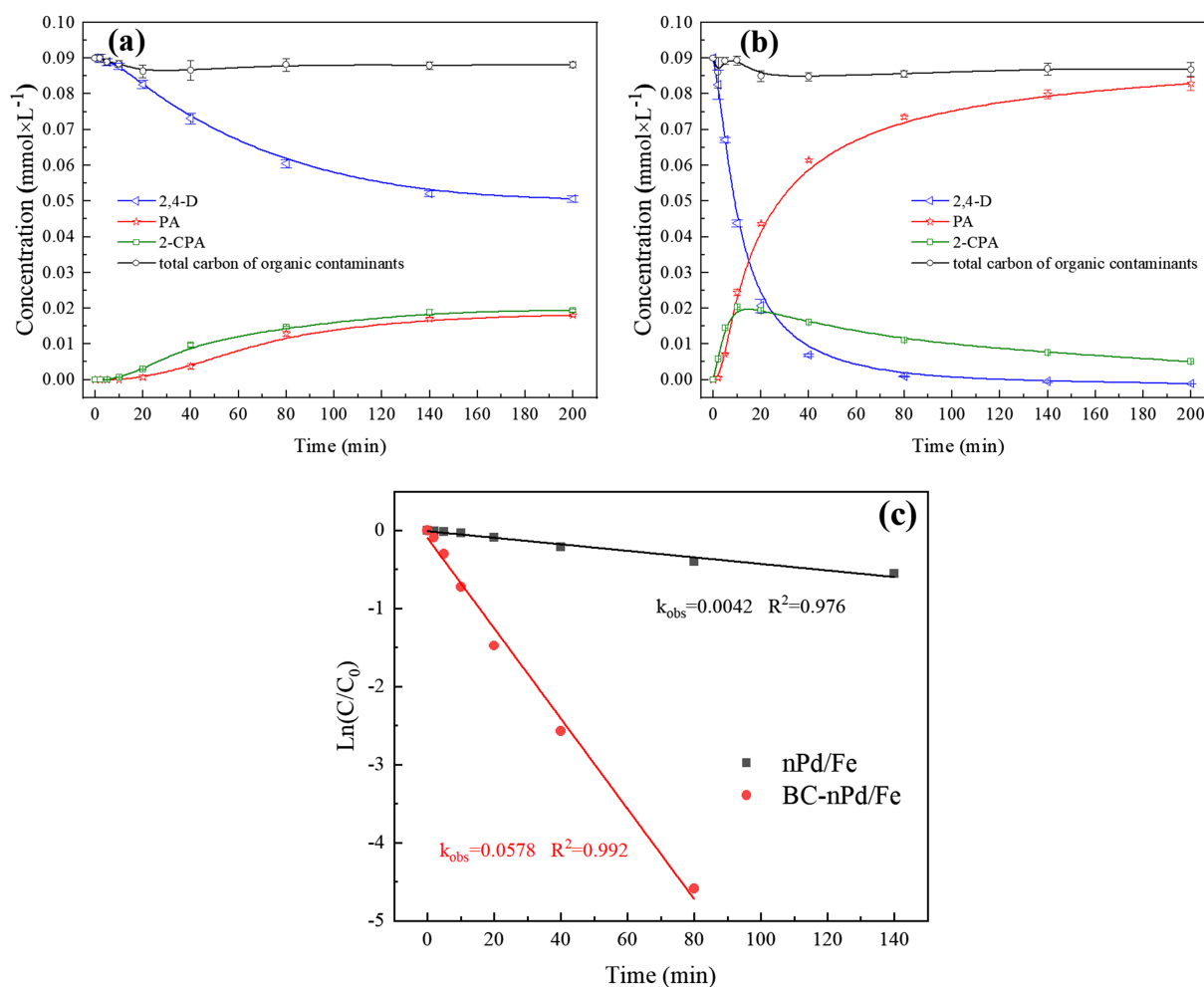
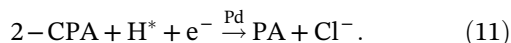
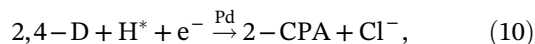
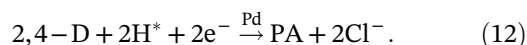


FIGURE 11 The dechlorination process of 2,4-D by (a) nPd/Fe and (b) BC-nPd/Fe and (c) the dechlorination kinetics of 2,4-D ($M_{\text{BC}}:M_{\text{Fe}} = 1:1$, $nZVI = 1.0 \text{ g L}^{-1}$, $C_{0,2,4-D} = 20.0 \text{ mg L}^{-1}$, $T = 25.0^\circ\text{C}$, $\text{pH} = 7.0$, $\text{Pd/Fe} = 0.5\%$, $n = 200 \text{ r min}^{-1}$). 2,4-D, 2,4-dichlorophenoxyacetic acid; BC-nPd/Fe, biochar-supported nano-palladium/iron; nZVI, nano-zero-valent iron

out that 2-CPA was temporarily formed before the final dechlorination product PA was generated. The entire dechlorination process can be represented by Equations 10, 11, and 12:



Overall reaction:



In these two systems, the total carbon from organic contaminants showed a similar trend. The total carbon loss from organic contaminants was approximately 2%–6% throughout the reaction. This small amount of loss

may be due to the adsorption of 2,4-D and its dechlorination products by BC or by the nonreactive sites or passivation layer on the surface of the particles.^[52,56] The carbon loss in the BC-nPd/Fe system, however, did not increase significantly (compared with nPd/Fe), as the total carbon loss of contaminants was 2.13% (in the nPd/Fe system) and 3.56% (in the BC-nPd/Fe system) at a reaction time of 200 min, respectively. It can be considered that the reductive dechlorination of 2,4-D was the main reaction process. In addition, the generation rate of the intermediate product 2-CPA was extremely low (4.3% in the BC-nPd/Fe system). Therefore, the concentration changes of 2,4-D and its final product PA can objectively reflect the dechlorination effect of BC-nPd/Fe on 2,4-D.

Figure 11c shows the kinetics of 2,4-D dechlorination, and the data fitted well with the pseudo-first-order model ($R^2 > 0.97$). The results demonstrated that the removal rate of 2,4-D by nPd/Fe and BC-nPd/Fe was controlled by the chemical reaction on the surface of the nanoparticles, which was consistent with the results

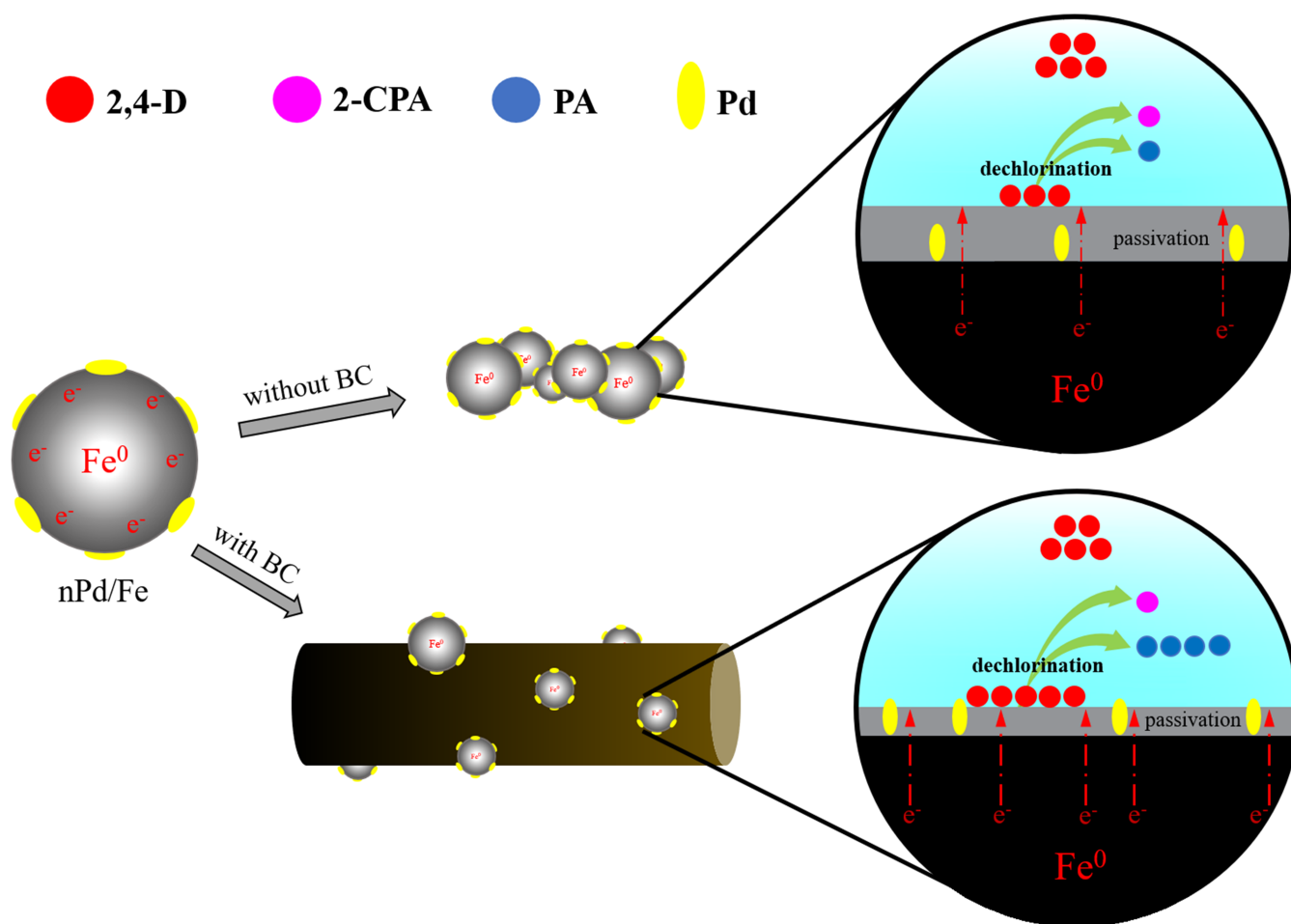


FIGURE 12 Mechanism of 2,4-D dechlorination by BC-nPd/Fe. 2,4-D, 2,4-dichlorophenoxyacetic acid; BC-nPd/Fe, biochar-supported nano-palladium/iron

discussed above. The k_{obs} values were significantly different in the nPd/Fe (0.0042 min) and BC-nPd/Fe (0.0578 min) systems; the latter was 13.8 times that of the former. The results clearly indicated that the presence of BC efficiently accelerated the rapid dechlorination of 2,4-D by nPd/Fe.

3.4 | Mechanism of 2,4-D dechlorination by BC-nPd/Fe

Figure 12 presents the reaction mechanism of 2,4-D by BC-nPd/Fe. During the dechlorination of 2,4-D, H_2 produced by the corrosion of nZVI was adsorbed by Pd and converted into H^* (Equations 7, 8, and 9). Then, the chlorine atoms in the 2,4-D molecule were substituted by H^* to form the intermediate 2-CPA and final product PA (Equations 10, 11, and 12). However, the generated Fe^{2+} may form a passivation layer covering the surface of the nPd/Fe particles during the nZVI corrosion process (Equations 5 and 6), which reduces the exposure of effective reaction sites on the particle surface, whereas the electron transfer between nZVI and contaminants is hindered. Therefore, the dechlorination efficiency of 2,4-D by nPd/Fe decreased rapidly.

When the supporting material BC was introduced, the agglomeration phenomenon between the nPd/Fe particles was significantly suppressed. Characterization analysis of BC-nPd/Fe composites revealed that nPd/Fe particles were dispersed and stabilized on the BC surface. Compared with nPd/Fe, the surface of the BC-nPd/Fe particles possessed more reactive sites and a larger contact area with the pollutant 2,4-D. In addition, BC inhibited the formation of a passivation layer on the nPd/Fe surface during the reaction (proved by XRD and XPS), which was beneficial to nZVI corrosion, H_2 dissociation, and electron transfer, thereby improving the efficiency and capacity to reduce 2,4-D by BC-nPd/Fe.

4 | CONCLUSION

In summary, BC prepared from peanut shells was found to be a good supporting multifunctional material for removing 2,4-D from water, and the characterization analyses indicated that the BC-nPd/Fe composites were successfully synthesized. SEM analysis revealed that nPd/Fe particles were well dispersed and stabilized on the surface of BC, and the average diameter of these particles was 88.8 nm. BET and VSM analyses indicated that the BC-nPd/Fe composites have a larger specific surface area and weaker magnetic properties as compared with nPd/Fe. XRD and XPS analyses showed that the surface

of BC-nPd/Fe particles retained a higher Fe^0 (8.1%) and Pd^0 (48.3%) content after the reaction, and the generation of a passivation layer was significantly suppressed, thus maintaining the high reduction reactivity of 2,4-D by BC-nPd/Fe during the reaction. The results also demonstrated that a higher weight ratio of BC to Fe and Pd loading, lower initial pH, suitable 2,4-D concentration, and reaction temperature were advantageous for the reductive dechlorination of 2,4-D by BC-nPd/Fe. Under optimal reaction conditions, the 2,4-D removal and PA generation rates increased from 44.1% and 20.1% (nPd/Fe) to 100.0% and 92.1% (BC-nPd/Fe), and the kinetic rate constant increased from 0.0042 to 0.0578 min, respectively. So this method might be a satisfactory approach if applied to treat the practical wastewater containing biologically resistant chlorinated-organics. Furthermore, the mechanism of 2,4-D removal by BC-nPd/Fe involved the corrosion of Fe^0 , and the generated H_2 , adsorbed by Pd, was converted into H^* , followed by a quick and efficient reduction of 2,4-D to PA because of the increased number of active sites and electron transfer. Thus, BC-nPd/Fe could be a promising composite material for the effective dechlorination of 2,4-D from a water environment.

ACKNOWLEDGMENT

The authors would like to acknowledge for the financial support from the National Natural Science Foundation of China (CN) [project no. 21477108].

AUTHOR CONTRIBUTIONS

Hongyi Zhou: Funding acquisition; project administration. **ning huang:** Investigation; visualization. **Yongkang Zhao:** Validation. **Junchao Xiang:** Data curation.

DATA AVAILABILITY STATEMENT

The data that support the findings of this study are available on request from the corresponding author. The data are not publicly available due to privacy or ethical restrictions.

ORCID

Hongyi Zhou  <https://orcid.org/0000-0001-5721-725X>

Ning Huang  <https://orcid.org/0000-0002-4639-2041>

REFERENCES

- [1] Z. M. Yang, X. H. Xu, M. Dai, L. Wang, X. S. Shi, R. B. Guo, *J. Hazard. Mater.* **2018**, 353, 490.
- [2] F. Islam, J. Wang, M. A. Farooq, M. S. S. Khan, L. Xu, J. W. Zhu, M. Zhao, S. Muños, Q. X. Li, W. J. Zhou, *Environ. Int.* **2018**, 111, 332.
- [3] N. Jaafarzadeh, F. Ghanbari, M. Ahmadi, *Chemosphere* **2017**, 169, 568.

- [4] E. I. Seck, J. M. Doña-Rodríguez, C. Fernández-Rodríguez, O. M. González-Díaz, J. Araña, J. Pérez-Peña, *Appl. Catal. B-Environ.* **2012**, *125*, 28.
- [5] M. A. Lemus, T. López, S. Recillas, D. M. Frías, M. Montes, J. J. Delgado, M. A. Centeno, J. A. Odriozola, *J. Mol. Catal. A-Chem.* **2008**, *281*, 107.
- [6] A. M. Smith, M. T. Smith, M. A. L. Merrill, J. Liaw, C. Steinmaus, *Ann. Epidemiol.* **2017**, *27*, 281.
- [7] D. Loomis, K. Guyton, Y. Grosse, F. E. Ghissasi, V. Bouvard, L. Benbrahim-Tallaa, N. Guha, H. Mattock, K. Straif, *Lancet Oncol.* **2015**, *16*, 891.
- [8] K. Shareef, G. Shaw, *Chemosphere* **2008**, *72*, 8.
- [9] S. González-Cuna, J. Galíndez-Mayer, N. Ruiz-Ordaz, S. Murugesan, *Int. Biodeterior. Biodegrad.* **2016**, *107*, 123.
- [10] Z. R. Sun, X. F. Wei, Y. B. Han, S. Tong, X. Hu, *J. Hazard. Mater.* **2013**, *244-245*, 287.
- [11] H. Chen, Z. L. Zhang, Z. L. Yang, Q. Yang, B. Li, Z. Y. Bai, *Chem. Eng. J.* **2015**, *273*, 481.
- [12] Y. J. Xiang, Z. Y. Xu, Y. Y. Zhou, Y. Y. Wei, X. Y. Long, Y. Z. He, D. Zhi, J. Yang, L. Luo, *Chemosphere* **2019**, *237*, 124464.
- [13] Y. J. Xiang, X. Yang, Z. Y. Xu, W. Y. Hu, Y. Y. Zhou, Z. H. Wan, Y. H. Yang, Y. Y. Wei, J. Yang, D. C. W. Tsang, *Sci. Total Environ.* **2020**, *709*, 136079.
- [14] F. B. Yao, Q. Yang, Y. Zhong, X. Y. Shu, F. Chen, J. Sun, Y. H. Ma, Z. Y. Fu, D. B. Wang, X. M. Li, *Water Res.* **2019**, *157*, 191.
- [15] X. Q. Li, D. W. Elliott, W. X. Zhang, *Crit. Rev. Solid State Mater. Sci.* **2006**, *31*, 111.
- [16] W. Zhang, C. B. Wang, H. L. Lien, *Catal. Today* **1998**, *40*, 387.
- [17] Y. J. Wu, J. H. Zhang, Y. F. Tong, X. H. Xu, *J. Hazard. Mater.* **2009**, *172*, 1640.
- [18] J. Fan, Y. Guo, J. Wang, M. Fan, *J. Hazard. Mater.* **2009**, *166*, 904.
- [19] G. C. C. Yang, H. L. Lee, *Water Res.* **2005**, *39*, 884.
- [20] Z. Q. Fang, X. H. Qiu, J. H. Chen, X. Q. Qiu, *Desalination* **2011**, *267*, 34.
- [21] S. Y. Oh, Y. D. Seo, K. S. Ryu, D. J. Park, S. H. Lee, *Environ Sci Process Impacts* **2017**, *19*, 711.
- [22] Y. Zhuang, S. Ahn, A. L. Seyfferth, Y. Masue-Slowey, S. Fendorf, R. G. Luthy, *Environ. Sci. Technol.* **2011**, *45*, 4896.
- [23] H. Y. Zhou, J. Han, S. A. Baig, X. H. Xu, *J. Hazard. Mater.* **2011**, *198*, 7.
- [24] Z. Q. Fang, X. H. Qiu, J. H. Chen, X. Q. Qiu, *J. Hazard. Mater.* **2011**, *185*, 958.
- [25] Y. J. Yu, Z. Huang, D. Y. Deng, Y. M. Ju, L. Y. Ren, M. D. Xiang, L. Z. Li, H. Li, *Chem. Eng. J.* **2017**, *325*, 279.
- [26] Y. Xu, W. X. Zhang, *Ind. Eng. Chem. Res.* **2000**, *39*, 2238.
- [27] D. O'Carroll, B. Sleep, M. Krol, H. Boparai, C. Kocur, *Adv. Water Resour.* **2013**, *51*, 104.
- [28] B. W. Zhu, T. T. Lim, *Environ. Sci. Technol.* **2007**, *41*, 7523.
- [29] C. B. Wang, W. X. Zhang, *Environ. Sci. Technol.* **1997**, *31*, 2154.
- [30] H. L. Lien, W. X. Zhang, *Appl. Catal. Environ.* **2007**, *77*, 110.
- [31] G. Huang, M. Wang, Y. Hu, S. Lv, C. Li, *PLoS ONE* **2017**, *12*, e0174589.
- [32] N. Sakulchaicharoen, D. M. O'Carroll, J. E. Herrera, *J. Contam. Hydrol.* **2010**, *118*, 117.
- [33] T. Wang, J. Su, X. Y. Jin, Z. L. Chen, *J. Hazard. Mater.* **2013**, *262*, 819.
- [34] B. Kakavandi, R. R. Kalantary, M. Farzadkia, *J. Environ. Health Sci.* **2014**, *12*, 115.
- [35] S. Nivedita, G. Vatsana, R. A. Singh, G. V. Kumar, S. Sarita, R. P. Kumar, *J. Environ. Chem. Eng.* **2018**, *6*, 5196.
- [36] Z. Li, S. Q. Luo, Y. Yang, J. W. Chen, *Chemosphere* **2019**, *216*, 499.
- [37] G. Sheng, A. Alsaedi, W. Shammakh, S. Monaqueul, J. Sheng, X. Wang, H. Li, Y. Huang, *Carbon* **2016**, *99*, 123.
- [38] X. S. Lv, X. Q. Xue, G. M. Jiang, D. L. Wu, T. T. Sheng, H. Y. Zhou, X. H. Xu, *J. Colloid Interface Sci.* **2014**, *417*, 51.
- [39] J. C. Yan, L. Han, W. G. Gao, S. Xue, M. F. Chen, *Bioresour. Technol.* **2015**, *175*, 269.
- [40] R. K. Xu, S. C. Xiao, J. H. Yuan, A. Z. Zhao, *Bioresour. Technol.* **2011**, *102*, 10293.
- [41] K. Weber, P. Quicker, *Fuel* **2018**, *217*, 240.
- [42] S. S. Wang, M. Y. Zhao, M. Zhou, Y. C. C. Li, J. Wang, B. Gao, S. Sato, K. Feng, W. Q. Yin, A. D. Igalavithana, P. Oleszczuk, X. Z. Wang, Y. S. Ok, *J. Hazard. Mater.* **2019**, *373*, 820.
- [43] E. J. Cole, O. R. Zandvakili, B. S. Xing, M. Hashemi, S. Herbert, H. H. Mashayekhi, *Data Brief* **2019**, *25*, 104073.
- [44] L. B. Qian, W. Y. Zhang, J. C. Yan, L. Han, Y. Chen, D. Ouyang, M. F. Chen, *Environ. Pollut.* **2017**, *223*, 153.
- [45] P. Devi, A. K. Saroha, *Chem. Eng. J.* **2015**, *271*, 195.
- [46] H. Choi, S. Agarwal, S. R. Al-Abed, *Environ. Sci. Technol.* **2009**, *43*, 488.
- [47] H. Li, Y. F. Qiu, X. L. Wang, J. Yang, Y. J. Yu, Y. Q. Chen, Y. D. Liu, *Chemosphere* **2017**, *169*, 534.
- [48] L. Han, J. C. Yan, L. B. Qian, W. Y. Zhang, M. F. Chen, *J. Environ. Manage.* **2019**, *245*, 238.
- [49] X. Shang, L. Yang, D. Ouyang, B. Zhang, W. Y. Zhang, M. Y. Gu, J. Li, M. F. Chen, L. H. Huang, L. B. Qian, *Chemosphere* **2020**, *249*, 126518.
- [50] D. Bhaduri, A. Saha, D. Desai, H. N. Meena, *Chemosphere* **2016**, *148*, 86.
- [51] H. Y. Zhou, J. C. Xiang, Y. K. Zhao, Y. Chen, *Sep. Purif. Technol.* **2018**, *207*, 377.
- [52] P. P. Wang, X. G. Liu, B. C. Yu, X. H. Wu, J. Xu, F. S. Dong, Y. Q. Zheng, *Sci. Total Environ.* **2020**, *702*, 134767.
- [53] N. S. Portillo-Vélez, R. Zanella, *Chem. Eng. J.* **2020**, *385*, 123848.
- [54] J. H. Ramirez, F. J. Maldonado-Hódar, A. F. Pérez-Cadenas, C. Moreno-Castilla, C. A. Costa, L. M. Madeira, *Appl. Catal. Environ.* **2007**, *75*, 312.
- [55] X. Wang, C. Chao, C. Ying, H. Liu, *J. Hazard. Mater.* **2009**, *161*, 815.
- [56] Y. J. Shi, H. D. Hu, H. Q. Ren, *Bioresour. Technol.* **2019**, *297*, 122281.

How to cite this article: Zhou H, Huang N, Zhao Y, Baig SA, Xiang J. Dechlorination of 2,4-dichlorophenoxyacetic acid using biochar-supported nano-palladium/iron: Preparation, characterization, and influencing factors. *Appl Organomet Chem.* 2020;e6010. <https://doi.org/10.1002/aoc.6010>